NANO LETTERS

2009
Vol. 9, No. 3
1127-1131

# Vortex Polarization States in Nanoscale Ferroelectric Arrays

**B. J. Rodriguez,[†,‡] X. S. Gao,[‡] L. F. Liu,[‡] W. Lee,[§] I. I. Naumov,[||] A. M. Bratkovsky,[||] D. Hesse,[‡] and M. Alexe*[,‡]**

*Max Planck Institute of Microstructure Physics, Weinberg 2, D-06120 Halle, Germany, Korea Research Institute of Standards and Science, Yuseong, 305-340 Daejon, Korea, and Hewlett-Packard Laboratories, 1501 Page Mill Road, Palo Alto, California 94304*

*Received December 4, 2008; Revised Manuscript Received January 15, 2009*



## ABSTRACT

**Two-dimensional arrays of ferroelectric lead zirconate titanate (PZT) nanodots were fabricated using pulsed laser deposition through ultrathin anodic aluminum oxide membrane stencil masks. The static distribution of polarization configurations was investigated using in- and out-of-plane piezoresponse force microscopy (PFM). The observed presence of an in-plane polarization component in nominally (001) oriented PZT suggests the existence of a significant deviation from the regular tetragonal structure that allows the formation of complex core-polarization states. Core-polarization states may indicate the presence of quasi-toroidal polarization ordering. The experimental results are compared with a theoretical model to determine the fingerprint of a vortex polarization state in PFM.**

The development of nanoferroelectrics,[1] driven primarily by the push for high-density nonvolatile memories[2,3] has spawned very active theoretical[4–7] and experimental[8] efforts toward understanding the predicted unusual (e.g., toroidal) phase transitions in low dimensional systems. Despite the predictions, and significant efforts at fabricating ferroelectric nanoislands via self-assembly[9–13] and stenciling[14–18] approaches, the experimental observation of a toroidal moment of polarization remains elusive. Recent theoretical considerations have reported that the existence of such polarization states depends on the size and shape of the nanodot and also on the strain and depolarizing field.[7] Armed with these guidelines for sample preparation, it should be possible to fabricate and observe ferroelectric nanoislands with novel polarization states given the appropriate visualization method. X-ray diffraction yields information on the crystallographic orientation but requires a large area array of similar nanodots. Transmission electron microscopy can reveal the polarization via the distortion of the unit cell but only provides one cross-section view of the nanodots and is inherently destructive. In contrast, piezoresponse force microscopy (PFM)[19–21] is ideally suited to investigate toroidal ordering within individual nanoferroelectric elements because it allows (a) the in- and out-of-plane polarization components to be measured locally and reconstructed to reveal the real-space polarization vector and (b) direct comparison with theory, as shown in this study.

Nanoferroelectrics have been studied extensively using PFM to address the superparaelectric limit[9,13] and other size effects[12,22] and to spatially resolve switching properties within individual ferroelectric nanodots[23] and at heterointerfaces in self-assembled multiferroic nanostructures.[24] Recently, Lee et al. used ultrathin anodic aluminum oxide (AAO) membranes as lift-off masks to fabricate single crystalline metal−ferroelectric−metal nanocapcitor arrays with near Tb in.$^{-2}$ density.[18] The Pt/Pb($Zr_{0.20}Ti_{0.80}$)$O_3$/Pt (PZT (20/80)) nanocapacitors grown on an MgO substrate were individually addressable by PFM and showed high-quality ferroelectric switching behavior. Similar PZT (20/80) nanostructures exhibited a−c domain patterns consistent with a low level of strain.[18] In this work, tetragonal PZT (40/60) nanostructures under compressive strain (and without top electrodes) are fabricated and investigated by PFM. In addition, recent theoretical data are analyzed to determine the signature of a vortex domain in a PFM experiment. The hallmark of toroidal ordering is then compared with experimentally obtained data.

An ultrathin AAO mask was prepared as described elsewhere[18] and transferred onto a pulsed laser deposition (PLD)-deposited 20 nm thick epitaxial $SrRuO_3$ film on a $SrTiO_3$ (100) substrate. PLD of PZT was performed by ablating a ceramic target with 10% PbO excess using a KrF excimer laser ($\lambda = 248$ nm) operated at an energy fluence of 1.0 mJ cm$^{-2}$ and a repetition rate of 5 Hz to deposit PZT

* Author to whom correspondence should be addressed, malexe@mpi-halle.mpg.de.
[†] Present address: Conway Institute of Biomolecular and Biomedical Research, University College Dublin, Belfield, Dublin 4, Republic of Ireland.
[‡] Max Planck Institute of Microstructure Physics.
[§] Korea Research Institute of Standards and Science.
[||] Hewlett-Packard Laboratories.

10.1021/nl8036646 CCC: $40.75 
**Published on Web 02/03/2009**

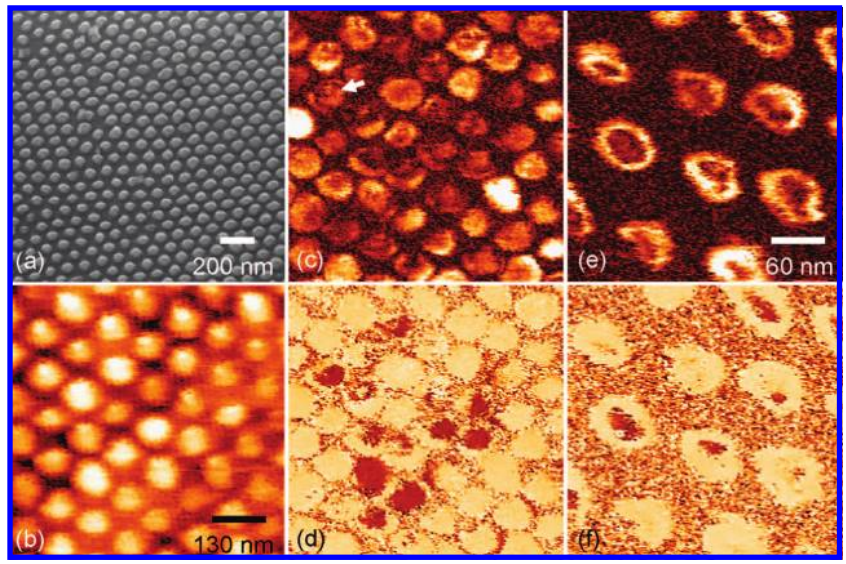


**Figure 1.** (a) SEM and (b) topography images of PZT (40/60) nanodot arrays. (c, d) VPFM amplitude and phase of the nanodot arrays shown in (b). (e, f) Higher resolution VPFM amplitude and phase images from another location within the nanodot array. The scale bar in (b) refers to (c) and (d), while the scale bar in (e) refers also to (f). The vertical data range in (b) is 18 nm.



(40/60) through the AAO stencil mask. PLD was performed in a low oxygen pressure of $1 \times 10^{-5}$ bar at a substrate temperature of 450 °C. The sample was subsequently annealed at 650 °C for 60 min in air, resulting in an ordered array of PZT nanostructures. Similarly grown nanostructures were revealed to be epitaxial from transmission electron microscopy images.[18] A scanning electron microscope (SEM) image of the PZT nanodot array is shown in Figure 1a. The periodicity of the pores is roughly 100 nm, and the corresponding average nanodot diameter and height are 50 and 20 nm, respectively.

PFM was performed using a commercially available atomic force microscope (AFM) (TM Microscopes, Auto-Probe CP Research) operated in contact mode. The piezoresponse signal was measured using a lock-in amplifier (DSP7260, Signal Recovery) and a $PtIr_5$-coated conducting AFM tip (ATEC-EFM, Nanosensors) with an elastic constant of about 2.5 N/m. Out-of-plane or vertical PFM (VPFM) was performed using a 25 kHz ac voltage, while in-plane or lateral PFM (LPFM)[9,25,26] was measured using a 6.75 kHz ac voltage applied to the tip.

Topography and VPFM amplitude and phase images of the PZT nanodot array are shown in Figure 1, panels b−d. The VPFM amplitude image provides information about the strength of the electromechanical coupling within each nanodot, while the VPFM phase image provides information regarding the orientation of the ferroelectric domains within each nanodot. Some dots are single domain and typically have higher piezoresponse signal, while other dots exhibit multidomain states in the VPFM phase image with corresponding domain walls in the VPFM amplitude image (e.g., arrow in Figure 1c). Higher resolution VPFM images from another area (Figure 1, panels e and f) clearly show the presence of ring or bubble domains, wherein the outer diameter of the dot corresponds to a negatively polarized domain (bright contrast in Figure 1f), and the inner portion is positively polarized (dark). The formation of this core-polarization state does not appear to be due to differences in crystallization, nor do we find evidence of chemical inhomogeneities in similarly prepared nanodots.[18] While an a−c domain configuration was observed in PZT (20/80) nanodots, no ring domains were observed.[18] Given the similar processing conditions and size of the nanodots, the ring-domain structure can be attributed to the differences in Zr/Ti composition and substrate-induced strain.

In order to understand the complex domain structure of these nanodots, it is necessary to measure both the LPFM and the VPFM signals from the same nanodots, as shown in Figure 2. From the VPFM images, single domain and multiple domain dots, including ring domains, can be observed. Similarly, both single and multiple domain configurations can be observed in the LPFM images. Clearly, there are several dots consisting of multiple domains with different in-plane components of polarization. Given the (001) orientation of the tetragonal PZT grown on $SrTiO_3$ (100), one would expect the measured in-plane component of polarization to be negligible in the absence of cross-talk.[27,28] This result indicates a deviation from the tetragonal structure[20] and may result from the presence of misfit dislocations[29] or the compositional proximity to the morphotropic phase boundary. It can be seen from the VPFM images that seemingly uniformly polarized dots can contain a single domain or multiple domains from the LPFM images. Dots exhibiting a ring-domain structure in the VPFM images can also be single domain in LPFM or can have a similar ring structure and vice versa. A visible ring structure in LPFM, ignoring any possible cross-talk effects due to the dot shape or size, or between the in- and out-of-plane components, does not correspond to a toroidal domain. The presence of different domain structures (single, bubble, etc.) within a single array with nanodots of similar geometry is an expected result, as the magnitude of the strain cannot be well-controlled. In fact, the multiple domain structure variants

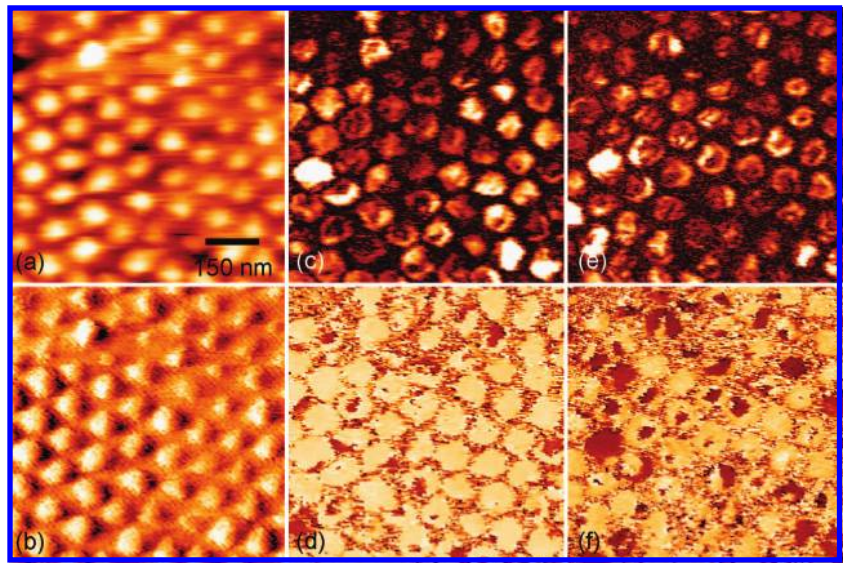


**Figure 2.** (a) Topography and (b) error signal images of a PZT (40/60) nanodot array. (c, d) VPFM and (e, f) LPFM amplitude and phase images from the location shown in (a, b). The scale bar in (a) refers to (b−f) as well. The vertical data range in (a) is 20 nm.



observed for similarly shaped nanodots is evidence that the contrast is not a result of edge or cross-talk effects.

Single and multiple vortex domains have been predicted for nanodots on the order of 16 nm in diameter and less or greater than 24 nm thick, respectively.[30] Ponomareva et al. have shown that close to open circuit electrical boundary conditions, at a critical value of the depolarization field, nanodots can undergo a transition from an out-of-plane polarization to a nonzero toroidal moment.[31] This transition implies the presence of one or the other type of polarization; however, in a recent paper by Naumov and Bratkovsky, intermediate phases are observed wherein a toroidal moment and an out-of-plane polarization coexist.[7] In Figure 3a−c, calculated polarization patterns are shown for 15.6 × 4 nm (diameter × height) PZT (50/50) nanodots with a compressive strain of −0.01 (Figure 3a) and in the stress-free, ground state (Figure 3b), and for a 7.6 × 2.4 nm nanodot under a compressive strain of −0.009 (Figure 3c). These data have been modeled using the piezoelectric surface approach,[32–36] wherein the angles between the polarization direction and the applied field and the scan orientation are used to construct *virtual* PFM images based on the calculated real-space polarization. Note that the piezosurface calculations are performed using piezoelectric coefficients for PZT (40/60),[37] the composition of the nanodot arrays investigated here. The experimentally obtained results can be compared to calculations for PZT (50/50) as both compositions are sufficiently close to the morphotropic phase boundary, where a mixing of allowed polarization directions may be present. Mixed VPFM and LPFM (*amplitude* × cos(*phase*)) maps for the three cases are shown in Figure 3, panels d−i. The virtual PFM maps for the 15.6 × 4 nm nanodot with a compressive strain of −0.01 are shown in Figure 3, panels d and g. The dot consists of stripe domains, and the in-plane response is zero. The ground-state, stress-free PFM maps (Figure 3, panels e and h) for the same sized dot reveal a toroidal ordering with an absence of an out-of-plane polarization. In panels f and i of Figure 3, PFM maps are shown for the 7.6 × 2.4 nm nanodot under a compressive strain of −0.009. In this case, a vortex polarization state coexists with an out-of-plane polarization taking the form of a core polarization or ring domain in VPFM. Additional maps are shown in the Supporting Information.

From these results, it is clear that the signature of a symmetric vortex domain can be described as having four quadrants (two zero, one positive, and one negative) in the LPFM map and zero VPFM signal; however, given the larger size of these nanodots, the experimental signature may be different. In the case of an intermediate state with the coexistence of a toroidal moment and an out-of-plane-polarization (Figure 3c), a ring or bubble domain can be observed in VPFM (Figure 3f). Clearly, the formation of a bubble domain is observed experimentally in these PZT (40/60) nanodots, and may be an indication of the presence of a toroidal moment. Bi-domain states consisting of two oppositely polarized coaxial cylindrical domains have been observed in magnetic systems where depolarizing field effects are weak,[38] and are therefore considered to be energetically unfavorable states in these nanodots. Ideally, the observation of a core-polarization would coincide with the signature predicted in Figure 3, panels f and i, but perhaps other variants exist as well. Shown in Figure 4, panels a–d, are VPFM and LPFM amplitude and phase images from a portion of the region shown in Figure 2. The VPFM images of dot 1 show a core-polarization state, but the LPFM images do not show the expected signature (Figure 3i). However, we should allow for the presence of more complicated, asymmetric, or pinched toroidal ordering. In fact, by comparing the data with the virtual PFM maps for just the top (0.4 nm thick) layer of simulated polarization (Figure 4, panels e and f) we see that the observed LPFM phase could be an indication of a toroidal ordering in the nanodot. Additional virtual PFM maps for different layers are shown in the Supporting Information. In this work, we assume the tip voltage is applied to the entire dot thickness and that the response from each unit cell layer contributes equally to the

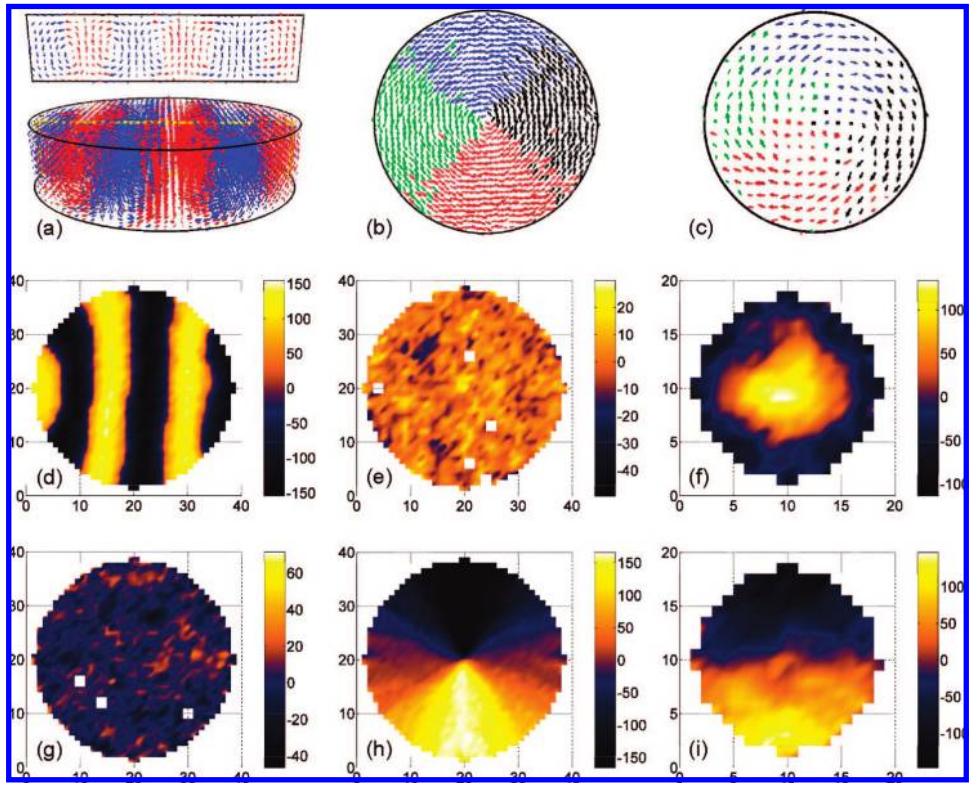


**Figure 3.** (a−c) Simulated polarization states and reconstructed (d−i) PFM maps. Polarization states for (a) the 15.6 × 4 nm nanodot with a compressive strain of −0.01, (b) the strain-free 15.6 × 4 nm nanodot, and (c) the 7.6 × 2.4 nm nanodot under a compressive strain of −0.009. (d, g) Mixed VPFM and LPFM images, respectively for (a). (e, h) VPFM and LPFM images of the dot depicted in (b). (f, i) VPFM and LPFM images of the 7.6 × 2.4 nm nanodot. The dimensions are given in the lattice parameter of the cubic bulk phase, a, in this case, 4.00 Å. In (b, c) the red, blue, green, and black arrows correspond to dipoles directed primarily along the [±100] and [0±10] directions. Panels a and b are reprinted with permission from ref 7 and are copyright (2008) by the American Physical Society.

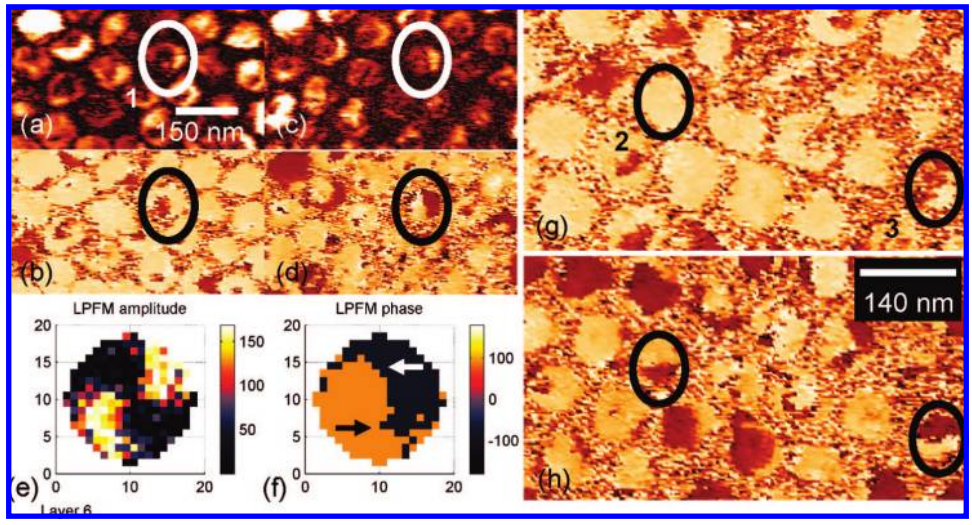


**Figure 4.** (a, b) VPFM and (c, d) LPFM amplitude and phase images, respectively of the same location (zoom-in of Figure 2). The circled dot shows a core-polarization state in VPFM. The LPFM images resemble the (e, f) virtual LPFM maps of the top layer of the simulated data. (g, h) VPFM and LPFM phase maps of a different location, with circled dots showing the signature of toroidal ordering in LPFM. The dimensions in (g, h) are given in the lattice parameter of the cubic bulk phase, *a*, in this case, 4.00 Å. The scale bar in (a) refers also to (b−d), and the scale bar in (h) refers to (g) as well.

piezoresponse signal. However, in LPFM, the top layers likely contribute more to the torsion of the cantilever through the friction force caused by shearing.

In Figure 4, panels g and h, VPFM and LPFM phase images from a different location are shown. Here, the LPFM phase reveals the expected toroidal signature in the circled dots, while the VPFM phase image reveals a single domain state in one case (dot 2) and an undetermined multidomain state in the other (dot 3). Again, while some models predict nanodots of certain geometry and strain will exhibit either

an in-plane vortex ordering or an out-of-plane polarization state, intermediate states have also been predicted, and a nanodot with the signature of toroidal ordering in LPFM and out-of-plane polarization may also be evidence of a vortex polarization state. Consider the precession of the polarization with an out-of-plane component as it curls slightly around the center of a nanodot. The projection of the in-plane component has toroidal ordering, while the out-of-plane piezoresponse remains nonzero, a signature which closely resembles the polarization state in dot 2.

In summary, we have used both experimental and theoretical approaches to reveal vortex polarization states in nanoscale ferroelectric arrays. Due in part to irregularities in shape and strain, nanodots with similar sizes may exhibit different domain structures. Scanning-related cross-talk effects related to the dot shape or size or between the in- and out-of-plane components of polarization may further impede the visualization of novel polarization states. Further improvements in stencil-assisted nanoferroelectric-array sample preparation may lead to precise control of strain and to polarization-state engineering. The described approach provides guidelines for visualizing the hallmark of toroidal ordering in nanoferroelectrics by PFM.

**Acknowledgment.** The authors acknowledge the financial support of the Volkswagen Foundation (Project I/80897) and the Alexander von Humboldt Foundation (B.J.R. and X.S.G.) and thank B. Birajdar for transmission electron microscopy analysis and S. Jesse for helpful discussions.

**Supporting Information Available:** Additional PFM maps. This material is available free of charge via the Internet at http://pubs.acs.org.

## References

(1) Scott, J. F. *J. Phys.: Condens. Matter* **2006**, *18*, R361.
(2) Scott, J. *Ferroelectric Memories*; Springer-Verlag: Berlin, 2000).
(3) Auciello, O.; Scott, J. F.; Ramesh, R. *Phys. Today* **1998**, *51*, 22.
(4) Ginzburg, V. L.; Gorbatsevich, A. A.; Kopayev, Y. V.; Volkov, B. A. *Solid State Commun.* **1984**, *50*, 339.
(5) Gorbatsevich, A. A.; Kopayev, Y. V. *Ferroelectrics* **1994**, *161*, 321.
(6) Naumov, I. I.; Bellaiche, L.; Fu, H. X. *Nature* **2004**, *432*, 737.
(7) Naumov, I.; Bratkovsky, A. M. *Phys. Rev. Lett.* **2008**, *101*, 107601.
(8) Gruverman, A.; Wu, D.; Fan, H.-J.; Vrejoiu, I.; Alexe, M.; Harrison, R. J.; Scott, J. F. *J. Phys.: Condens. Matter* **2008**, *20*, 342201.
(9) Roelofs, A.; Schneller, T.; Szot, K.; Waser, R. *Appl. Phys. Lett.* **2002**, *81*, 5231.
(10) Szafraniak, I.; Harnagea, C.; Scholz, R.; Bhattacharyya, S.; Hesse, D.; Alexe, M. *Appl. Phys. Lett.* **2003**, *83*, 2211.
(11) Nonomura, H.; Nagata, M.; Fujisawa, H.; Shimizu, M.; Niu, H.; Honda, K. *Appl. Phys. Lett.* **2005**, *86*, 163106.
(12) Ahn, S. H.; Jung, W. W.; Choi, S. K. *Appl. Phys. Lett.* **2005**, *86*, 172901.
(13) Rüdiger, A.; Schneller, T.; Roelofs, A.; Tiedke, S.; Schmitz, T.; Waser, R. *Appl. Phys. A: Mater. Sci. Process.* **2005**, *80*, 1247.
(14) Shin, H.-J.; Choi, J. H.; Yang, H. J.; Park, Y. D.; Kuk, Y.; Kang, C.-J. *Appl. Phys. Lett.* **2005**, *87*, 113114.
(15) Ma, W.; Harnagea, C.; Hesse, D.; Gösele, U. *Appl. Phys. Lett.* **2003**, *83*, 3770.
(16) Ma, W.; Hesse, D. *Appl. Phys. Lett.* **2004**, *84*, 2871.
(17) Lee, S. K.; Lee, W.; Alexe, M.; Nielsch, K.; Hesse, D.; Gösele, U. *Appl. Phys. Lett.* **2005**, *86*, 152906.
(18) Lee, W.; Han, H.; Lotnyk, A.; Schubert, M. A.; Senz, S.; Alexe, M.; Hesse, D.; Baik, S.; Gösele, U. *Nat. Nanotechnol.* **2008**, *3*, 402.
(19) Gruverman, A.; Auciello, O.; Tokumoto, H. *Annu. Rev. Mater. Sci.* **1998**, *28*, 101.
(20) Kalinin, S. V.; Rodriguez, B. J.; Jesse, S.; Karapetian, E.; Eliseev, E. A.; Morozovska, A. N. *Annu. Rev. Mat. Res.* **2007**, *37*, 189–238.
(21) Kalinin, S. V.; Rodriguez, B. J.; Jesse, S.; Shin, J.; Baddorf, A. P.; Gupta, P.; Jain, H.; Williams, D. B.; Gruverman, A. *Microsc. Microanal.* **2006**, *12*, 206–20.
(22) Chu, M.-W.; Szafraniak, I.; Scholz, R.; Harnagea, C.; Hesse, D.; Alexe, M.; Gösele, U. *Nat. Mater.* **2004**, *3*, 87.
(23) Rodriguez, B. J.; Jesse, S.; Alexe, M.; Kalinin, S. V. *Adv. Mater.* **2008**, *20*, 109.
(24) Rodriguez, B. J.; Jesse, S.; Baddorf, A. P.; Zhao, T.; Chu, Y. H.; Ramesh, R.; Eliseev, E. A.; Morozovska, A. N.; Kalinin, S. V. *Nanotechnology* **2007**, *18*, 405701.
(25) Eng, L. M.; Abplanalp, M.; Günter, P. *Appl. Phys. A: Mater. Sci. Process.* **1998**, *66*, S679.
(26) Eng, L. M.; Güntherodt, H. J.; Schneider, G. A.; Köpke, U.; Muñoz Saldaña, J. *Appl. Phys. Lett.* **1999**, *74*, 233.
(27) Peter, F.; Rüdiger, A.; Waser, R.; Szot, K.; Reichenberg, B. *Rev. Sci. Instrum.* **2005**, *76*, 046101.
(28) Jungk, T.; Hoffmann, Á.; Soergel, E. *Appl. Phys. Lett.* **2006**, *89*, 042901.
(29) Du, X.-H.; Zheng, J.; Belegundu, U.; Uchino, K. *Appl. Phys. Lett.* **1998**, *72*, 2421.
(30) Wang, J.; Kamlah, M.; Zhang, T.-Y.; Li, Y.; Chen, L.-Q. *Appl. Phys. Lett.* **2008**, *92*, 162905.
(31) Ponomareva, I.; Naumov, I. I.; Kornev, I.; Fu, H.; Bellaiche, L. *Phys. Rev. B* **2005**, *72*, 140102.
(32) Du, X.; Belegundu, U.; Uchino, K. *Jpn. J. Appl. Phys., Part 1* **1997**, *36*, 5580.
(33) Du, X.; Zheng, J.; Belegundu, U.; Uchino, K. *Appl. Phys. Lett.* **1998**, *72*, 2421.
(34) Du, X.; Wang, Q.-M.; Belegundu, U.; Bhalla, A.; Uchino, K. *Mater. Lett.* **1999**, *40*, 109.
(35) Kalpat, S.; Du, X.; Abothu, I. R.; Akiba, A.; Goto, H.; Uchino, K. *Jpn. J. Appl. Phys., Part 1* **2001**, *40*, 713.
(36) Harnagea, C.; Pignolet, A.; Alexe, M.; Hesse, D. *Integr. Ferroelectr.* **2001**, *38*, 23.
(37) Haun, M. J.; Furman, E.; Jang, S. J.; Cross, L. E. *Ferroelectrics* **1989**, *99*, 63.
(38) Hehn, M.; Ounadjela, K.; Bucher, J.-P.; Rousseaux, F.; Decanini, D.; Bartenlian, B.; Chappert, C. *Science* **1996**, *272*, 1782.

NL8036646